Deformation of loops in 2D packing of flexible rods

T A Sobral[1,2], V H de Holanda[1,3], F C B Leal[1], T T Saraiva[1,4]

[1] Departamento de Física, Universidade Federal de Pernambuco, 50670-901, Recife, Brazil

[2] Instituto Federal de Educação, Ciência e Tecnologia do Rio Grande do Norte, RN 288, s/n, Nova Caicó, 59300-000 - Caicó, Brazil

[3] Instituto Federal de Educação, Ciência e Tecnologia do Sertão Pernambucano, PE, Zona Rural, 56915-899 - Serra Talhada, Brazil

[4] National Research University Higher School of Economics, 101000, Moscow, Russia

E-mail: tteixeirasaraiva@hse.ru; thiago.sobral@ifrn.edu.br

15 December 2020

Abstract. The injection of a long piece of flexible rod into a two-dimensional domain yields a complex pattern commonly studied through elasticity theory, packing analysis, and fractal geometries. "Loop" is an one-vertex entity which which is naturally formed in this system. The role of the elastic features of each individual loop in 2D packing has not yet been discussed. In this work we point out how the shape of a given loop in the complex structure allows to estimate local deformations and forces. First, we build sets of symmetric free loops and performed compression experiments. Then, tight packing configurations are analyzed by using image processing. We found that the dimensions of the loops, confined or not, obey the same dependence on the deformation. The result is consistent with a simple model based on 2D elastic theory for filaments, where the rod adopts the shape of Euler's elasticas between its contact points. The force and the stored energy are obtained from numerical integration of the analytic expressions. In an additional experiment, we obtain that the compression force for deformed loops corroborates the theoretical findings. The importance of the shape of the loop is discussed and we hope that the theoretical curves may allow statistical considerations in future investigations.

Keywords: elasticity, elastic loops, elastica, packing, pattern formation

1. Introduction

The injection of filaments into cavities is a basic problem involving elasticity and self-exclusion. These are two aspects of great importance in nature, with wide range of influence from polymeric packing [1, 2] to DNA packaging in viral capsids [3, 4, 5, 6]. The structures formed by the confinement of wires packaged [3, 7] and crumpled surfaces [8] present anomalous characteristics [3] that are of interest to soft matter physics and statistical physics. The mechanical properties are influenced by the hierarchy of its

folds [9, 10] and show a behavior similar to that found in unbranched polymers diluted in a solvent [2]. We focus on the two-dimensional confinement of an elastic slender rod, which present interesting scaling properties [11], energy distributions [12, 13, 10], and morphological phases [14]. The rigidity of the structure [3] is of particular interest in the present study.

In a typical 2D confinement as show in Fig. 1(a), the formation of self-contact points divides the area of the cavity into cells with variable number of vertexes. "Loop" is the term used to designate single-vertex cells [9], as those highlighted in Fig. 1(b). The determination of the loops allows to identify the points of higher curvatures [15] and helps to determine the morphology of the complex pattern [14]. The key concept here is *curvature*, which links our work to the physics of pattern formation in protein chains and membranes [16] and, not less astonishingly, quantum gravity [17]. In addition, the number of loops gives the jamming length and the dynamic state of the system [18, 19]. Note that the type of loops studied here, in which curvature reverses sign along its length, can be unstable or less frequent in the case of 3D confinements, where torsion may have a major influence and the curvature maintains constant sign [20]. Despite this intrinsic relevance, the shape of the conforming loop has been little studied. Here, we report a set of three experiments and a model that describes the deformations of the loop. The main objective is identifying physical quantities in the complex confined system by analyzing the shape of a single loop.

The article is organized as follows: in Sec. 2, we show our measurements of fundamental geometric quantities of single loops under compression and compare them to case of loops from a packed conformation of longs rod inside 2D circular and rectangular cavities; in Sec. 3, one can find solutions for the elasticity equation in 2D for the loop under compression; in Sec. 4, it is described the experiment for measuring the force of compressing and stretching the loops in the configurations obtained in the previous section; and in Sec. 5, we show our conclusions.

2. Packing and compression of elastic loops

We built elastic loops from rods and ribbons and compared them with loops in the packing of a single filament into circular and rectangular cavities. We observed that, under compression, the dimensions of the loops vary according to the same curve irrespective of confinement. From this result we propose how to infer local information in complex patterns from simple analysis of shape and size of loops. The theoretical description follows the elastic model for filaments [21, 22, 23], and allows us to determine the shape of the loops, as well as the force and stored energy.

The objective of the first experiment is determining the mechanical response of a single loop under compression. The loops were constructed by bending a piece of rod in order to merge the ends into a vertex point. A bent rod leaves the planar configuration when the ends are close to each other [23, 24], then transparent parallel plates are used to constraint it. The rods used are either nylon fishing lines of 0.80 mm of diameter

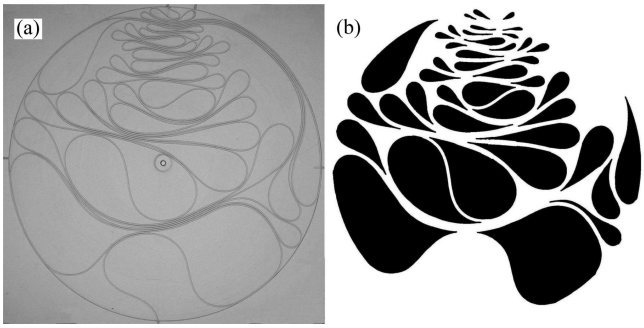

Figure 1. (a) The packing of a 1 mm thick nylon fishing line into a circular cavity with diameter of 200 mm. (b) The loops (in black) are closed domains with one vertex.

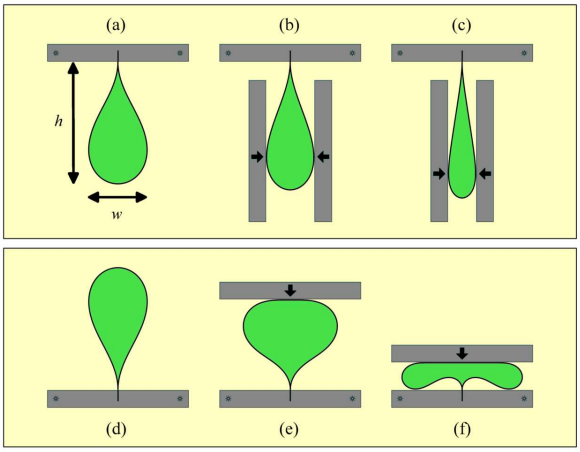

Figure 2. Superior view of deformed loops: (a-c) compressing sideways by imposing smaller widths, and (d-f) compressing along the symmetric axis by imposing smaller heights.

or polymeric tubes of 5.0(2.5) mm of outer (inner) diameter. The constraint plates are made of acrylic with a thickness of 1.0 cm. We also construct planar loops from ribbons with width 1.0 cm, and made of either A4 paper or transparent Mylar sheets. An interesting point is that loops made from ribbons with large width are naturally planar [20], and have the advantage of eliminating friction effects due to contact with parallel plates.

The initial conformation is denominated "free loop". The perimeter $\lambda = \lambda_0$ is defined when the flexible rod or ribbon is straight, and was chosen randomly in an interval $\lambda_0 = \{97-366\}$ mm. The loops are large in order to avoid plasticity effects. The height h of the loop is defined along its symmetric axis as the distance from the vertex to the top of the bulge. Perpendicularly, the largest width of the loop is w [Fig. 2(a)]. Both h and w are measured with a digital caliper. The initial ratios $h_0/\lambda_0 = (0.424 \pm 0.007)$ and $w_0/\lambda_0 = (0.210 \pm 0.008)$ are essentially the same irrespective the type or material. For rods, we measured the dimensions h_0 and w_0 from the neutral axis.

The experiment consists of compressing the loop along two perpendicular axis

(Fig. 2). In the first part, the loop is compressed between two parallel aluminum plates, requiring w to decrease as illustrated in Fig. 2(a-c). Care is taken in order to preserve the loop as symmetric as possible. The system responds by increasing the height h. The compressing continues until the physical limit $w \to 0$ which leads to $h \to \lambda/2$. During this process, the contact points between the loop and the compression plates move downwards as indicated by small arrows in Fig. 2(b-c). In the second part of the experiment, the loop is compressed between two parallel aluminum plates, requiring h to decrease as illustrated in Fig. 2(d-f). In this case, the system responds by increasing w. The compressing continues until the physical limit $h \to 0$ which leads to $w \to \lambda/2$. The experiment is performed horizontally over a table without gravitational effects.

The results of the experiment illustrated in Fig. 2 are shown in Fig. 3(a-b) as a $h \times w$ diagram, normalized by λ. The diagram is identical for loops built from ribbons (Fig. 3a) and rods (Fig. 3b), and agrees with the theoretical description (solid line) based on Euler's elastica which we discuss afterwards. The values for the free loop are indicated by a big cross. Since compressing w leads to higher h, the graph in Fig. 3(a-b) must be read from the cross to the left. On the other hand, compressing h leads to higher w, and the graph in Fig. 3(a-b) must be read from the cross to the right. Therefore, the range of the data shown in the Fig. 3(a-b) covers the entire physical domain, from values of dimensions for the free loop to completely crushed shapes.

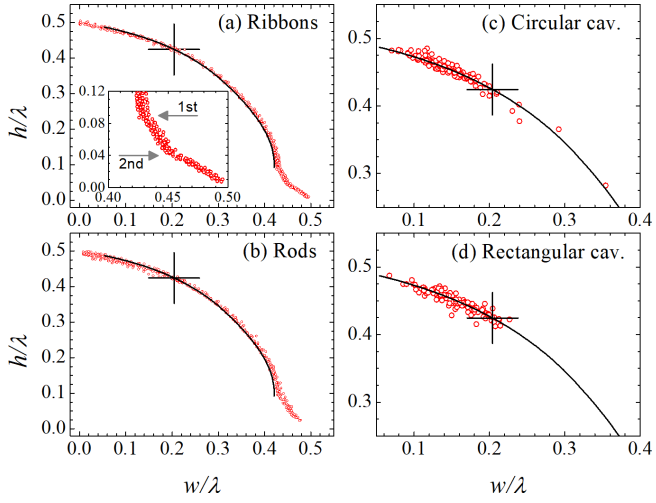

Figure 3. The $h \times w$ diagram for deformed loops made of (a) ribbons, and (b) fishing lines. With image processing, loops are obtained from (c) the packing of a nylon fishing line into circular cavities, and (d) the packing of a tubular rod into rectangular cavities. The big cross indicates the sizes of the free loop. The solid line is obtained from the theoretical reasoning. See text for more details.

The free loop has an anisotropic shape and its response to compression is different depending on the load axis. While the reduction in w leads to an increase in h until the physical limit $h \to \lambda/2$, a reduction in h leads to an increase in w until a limited value, $w \to w_m = (0.429 \pm 0.005)\lambda$. If the compression continues beyond this point, the curve follows towards the physical limit $w \to \lambda/2$ with two discontinuities in its

slope [see inset in Fig. 3(a)]. The first discontinuity, at $h = (0.089 \pm 0.002)\lambda$, is due to the emergence of new contact points between the loop and the plates as shown in Fig. 2(f). The second discontinuity, at $h = (0.042 \pm 0.002)\lambda$, is due to the emergence of two self-contact points which divides the loop into three shapes: one curved triangle between two small loops.

In order to study the problem of 2D confining, the flexible rod can be split at the contact points into pieces that are treatable numerically with Euler's equation [25, 10]. The problem is complex due to the fractal distribution of contact points [15]. It has been discussed whether self-contacts define arcs of propagating forces across the structure [15, 14]. Here, on the other hand, we focus on the shape of the loops as a guide to access both qualitative and quantitative information about local deformations and energy. The second experiment consists in the two-dimensional injection of thin rods into planar slender cavities. The objective is to analyze how the loops, which are naturally formed in the confinement, behave in light of the $w \times h$ diagram. This experiment is also divided in two parts. In the first one, nylon fishing lines with a diameter of 1.0 mm are injected into circular cavities with 201 mm in diameter as shown in Fig. 1(a). In the second part of the experiment, polymeric tubular rods with 50 mm in diameter are injected into rectangular cavities of 400×200 mm^2 as illustrated in Fig. 4(a). All injections are performed manually into a dry cavity, free of lubricants, in a rate about 1 cm/s. The injection stops when the system jams due to the rigidity around the injection channel.

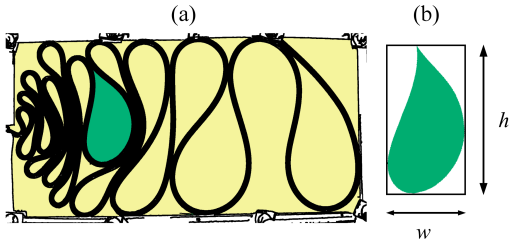

Figure 4. (a) Digital image of the tight packed flexible tube of 50 mm in diameter inside a rectangular cavity of 200×400 mm^2. (b) Each loop is framed inside a rectangle which defines h and w (see text for details).

The particular conformation presented in Fig. 4(a) is chosen as a representative case where we can briefly discuss the role of the elasticity, self-exclusion, and friction with the cavity. The first loops that formed are pushed away from the injection channel, shown in the right region of Fig. 4(a). These loops are larger, and requires low values for the injection force in the early stages. Observe that the shape of the loops are prevented from changing due to the contacts with the cavity and friction. The rod has small self-contact regions, and the stacked loops transmit the force through the system by compressing each other. The geometric pattern and local rigidity are then governed by the elasticity of the loops. On the other hand, the last loops are close to the injection channel, see left region of Fig. 4(a). The injection force in this stage is higher,

which reduces the perimeter of the loops and limits them to occupy the periphery of the pattern, without contacting the cavity. The rod has large self-contact regions that transmit the force through the system. In the case shown in Fig. 4(a) the loops are compressed by neighbors in a configuration that resembles Fig. 2(a-c). In a cavity of generic shape, however, we expect that the loops can interact also as in Fig. 2(d-f). For example, there are differences between patterns generated from circular and rectangular cavities [Compare Fig. 1(a) and Fig. 4(a)].

In order to construct a $h \times w$ diagram for loops inside cavities, we need to measure its dimensions non-invasively. We can select the loops by image processing [Fig. 4(a)]. However, the loops interact in a complicated manner and assume non-symmetric shapes, so that we need to revise the definitions of h and w. We focus here on the reading of the geometric pattern by prioritizing simple definitions. First, the selected loop is inscribed into a rectangle. Rotating the loop will change the aspect ratio of the frame. The chosen angle is that which maximizes the height of the frame, as shown in Fig. 4(b). This dimension is identified as h or w accordingly to the position of the tip and the bulge of the loop. Following this procedure, all symmetrical loops illustrated in Fig. 2 maintain their dimensions. The points at the edge of the loop are interpolated by a curve that allows us to measure the dimensions h, w, and λ with the same units. Such method is repeated for each loop in the image. The result is shown in Fig. 3(c) for loops inside circular cavities, and in Fig. 3(d) for loops inside rectangular cavities.

The main result in Fig. 3 is that the loops obtained from injection of rods (c and d) present the same behavior as the loops outside the cavities (a and b). However, the data from packed loops distribute themselves majoritarily in the left side of the diagram, instead of spreading over the whole diagram. This is in agreement with the fact that the loops are aligned perpendicular to the injection channel. The injection force then acts to compress the loops laterally, reducing both their perimeter and width. However, Fig. 3(c) shows that few loops are also longitudinally compressed in circular cavities. In this cavity rotation and slippage are more accessible than in the rectangular one. In the general sense, this confirms that the way at which the loops populate the diagram depends on the shape and size of the cavity.

3. Theoretical description

Let us begin our reasoning by considering the free loop. Between contact points, the vector force is fixed along the arc length s of the rod, $\mathbf{F}(s) = P\hat{\mathbf{i}}$. Therefore, the shape is governed by infinitesimal torques $d\Gamma(s) = F \sin\theta \, ds$, where θ is the angle between $d\mathbf{s}$ and the direction of the force $\mathbf{F}$. The torque is related to the local curvature, $\Gamma(s) = -\mu \frac{d\theta}{ds}$, where μ is the bending rigidity. We can write

$$\frac{d^2\theta}{d\tilde{s}^2} = -\sin\theta, \tag{1}$$

where the tilde over any quantity q means $\tilde{q} \equiv q\sqrt{F/\mu}$. The coordinates are given by integration of $d\tilde{x}(\tilde{s})/d\tilde{s} = \cos\theta$ and $d\tilde{y}(\tilde{s})/d\tilde{s} = \sin\theta$. The general solutions are

obtained in terms of elliptic integrals and elliptic functions, and the overall shape is determined by the elliptic parameter p [22]. The free loop corresponds to the elastica with a self-contact point, at $\tilde{s} = \tilde{s}^*$, in which the following conditions hold

$$\tilde{x}(\tilde{s}^*) = \tilde{x}(0) \quad \text{and} \quad \left.\frac{d\tilde{x}(\tilde{s})}{d\tilde{s}}\right|_{\tilde{s}=\tilde{s}^*} = 0. \tag{2}$$

The outcome is a numeric equation for p whose solution is $p^* = 0.731183$ [22]. We determine λ, h, and w by computing the vertex point and the points of maximum. We find $h_0/\lambda = 0.424308$ and $w_0/\lambda = 0.204214$, irrespective of the bending rigidity. These values are in agreement with the experimental finding, then we can state that the self-touching elastica describes quite well the shape of the free loop.

Our model for a general symmetric loop requires attention to points where an external force acts to deform the loop. We assume here that the lateral compression of the loop is equivalent to a longitudinal stretching. In this manner, all compression in Fig. 2 can be described by the application of a single normal force $\mathbf{N} = N\hat{\mathbf{j}}$ at the middle point of the loop. The loop is thus composed of mirrored elasticas. The total force becomes $\mathbf{F} = P\hat{\mathbf{i}} + N\hat{\mathbf{j}}$ and the reference line of the elasticas changes from the horizontal to an oblique direction, whose angle is $\gamma_0 \equiv \tan^{-1}(N/P)$. Eq. 1 remains valid, but the contour conditions (Eq. 2) are adapted for rotated coordinates. Then, we obtain a numeric equation for p whose solution now depends on the angle γ_0. Figs. 5(a-f) show how two symmetrical elasticas merge in order to compose the deformed loop. Fig. 5(g) shows how the self-touching condition changes the elliptic parameter as a function of the angle γ_0.

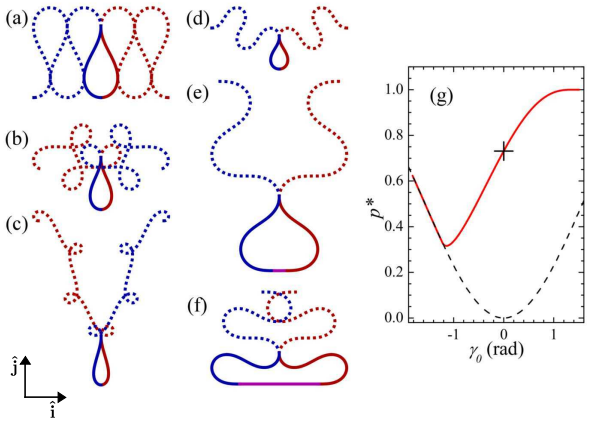

Figure 5. The symmetric loop is composed of two elasticas (a-f) rotated respectively by $\gamma_0 = \{0, 0.60, 1.20, -0.55, -1.27, -1.82\}$ rad. (g) p^* dependence with the compression force through γ_0. The dashed line corresponds to $\dot{\gamma}_0 = 0$ case. See text for details.

The free loop corresponds to $\gamma_0 = 0$ and it is illustrated in Fig. 5(a). In the stretching case $\gamma_0 > 0$, the elliptic parameter increases [Fig. 5(g)] and the elasticas have pieces that cross each other, as shown in Fig. 5(b-c). In the compressing case $\gamma_0 < 0$, the elliptic parameter decreases [Fig. 5(g)] and the elasticas have no crossing points, as shown in Fig. 5(d-f). The dashed line in Fig. 5(g) shows where the contact point in the

bulge has null curvature, and corresponds to $p^* = \sin^2(\gamma_0/2)$. Because the compressing plate does not allow convex curvature, the contact region becomes a straight line which extends itself between two inflectional points. From this simple model, we can determine the lengths λ, h and w, as shown by solid lines in Fig. 3.

The agreement between the theoretical curve and the experimental data (Fig. 3) shows the relevance of this purely elastic model. Furthermore, we can calculate the force associated with a given shape, $F = \mu(\tilde{s}/s)^2$. The result for the force is shown in Fig. 6 and (inset) the energy cost of deformation $\Delta E = W = \int \mathbf{N}\cdot d\mathbf{h}$. Big crosses in that figure indicate the values for the initial condition.

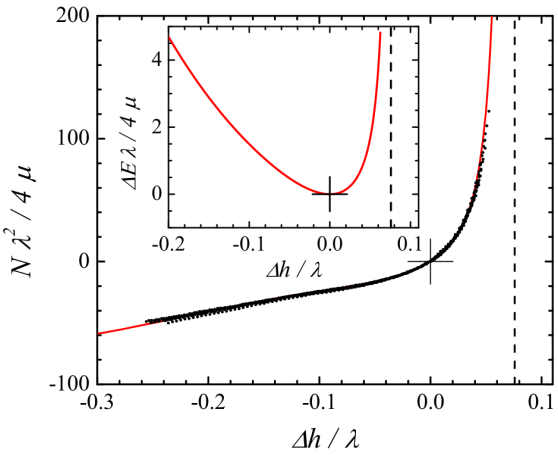

Figure 6. The force N and (inset) the stored energy E as functions of the deformation $\Delta h/\lambda$ for purely elastic loops. Black points corresponds to experimental data. Dashed lines indicate the physical limit of deformation. See text for details.

4. Measuring the force for compression and stretching of loops

In order to measure the force N, a dynamometer is attached to the vertex of the loop, which is arranged in a horizontal plane (see Fig. 7(a)). The compression part ($N < 0$) is performed by pushing the bulge against a fixed wall, while the stretching ($N > 0$) is done by fixing the bulge with a metal hook and then lengthen the loop by pulling the dynamometer (see Fig. 7(b)). The measurements of the force (N) versus deformation ($\Delta h/\lambda$) were obtained with an automatic equipment of instrumental precision of 1 cN. The space steps were of 2 mm, and 10 different ribbons of Mylar sheets were used. The result for the normal force is shown as black points in Fig. 6(b). Due to asymmetry, the force is greater when the loop is stretched than when it is compressed by a same extension. The dashed line in Fig. 6 shows the limit $h \to \lambda/2$, where force and energy diverge because small radius of curvature. The agreement between model and experiment allows us to estimate both the force and stored energy for loops inside complex patterns.

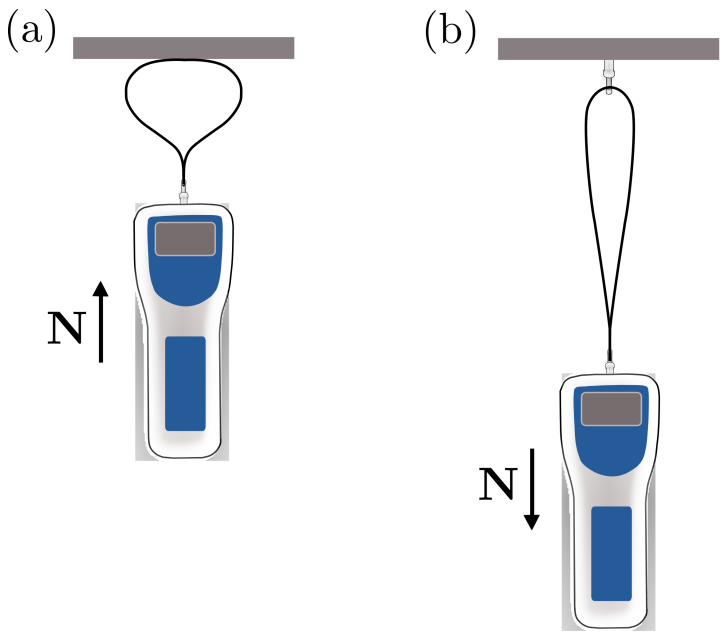

Figure 7. Schemes of the measurements of the force N (a) to compress the loop and (b) to stretch the loop. This experiment was executed along the horizontal plane perpendicular to the gravitational force.

5. Conclusion

In this work we suggest new methods to analyze the deformation of a flexible rod packed into a 2D cavity. The $h \times w$ diagram in Fig. 3 enable us to calculate the perimeter of the loops and their deformation level, compared to a simple model based on the Euler's elastica [22]. The purely elastic case is an important reference [12, 26], and the graphs in Fig. 6 allow us to estimate the forces and stored energy in any loop immersed in a complex pattern. In this physical system, friction and plasticity play very important roles [14, 13], but the effect on each loop needs further attention. Finally, the results of the dependence of the stored energy on the loop deformation open up new possibilities for application of statistical techniques to 2D confining of flexible rods.

Acknowledgments

We acknowledge Professor Eduardo O. Dias from UFPE for fruitful discussions. The present work was supported by CNPq, Conselho Nacional de Desenvolvimento Científico e Tecnológico, Brazil (numbers 157218/2012-0, 141813/2016-4, and 152053/2016-6).

References

[1] Paul J. Flory. *Principles of polymer chemistry.* Cornell University Press, 1953.
[2] Pierre-Gilles de Gennes. *Scaling concepts in polymer physics.* United Kingdom by Cornell University Press Ltd., Ithaca, United States, first edition, 1979.

[3] M A F Gomes, V P Brito, A S O Coelho, and C C Donato. Plastic deformation of 2d crumpled wires. *Journal of Physics D: Applied Physics*, 41(23):235408, 2008.

[4] N. Stoop, J. Najafi, F. K. Wittel, M. Habibi, and H. J. Herrmann. Packing of elastic wires in spherical cavities. *Phys. Rev. Lett.*, 106:214102, May 2011.

[5] Roman Vetter, Falk K Wittel, and Hans J Herrmann. Morphogenesis of filaments growing in flexible confinements. *Nature communications*, 5, 2014.

[6] V. H. de Holanda and M. A. F. Gomes. Scaling, crumpled wires, and genome packing in virions. *Phys. Rev. E*, 94:062406, Dec 2016.

[7] M. A. F. Gomes, F. F. Lima, and V. M. Oliveira. Plastic properties of crumpled wires. *Philosophical Magazine Letters*, 64(6):361–364, 1991.

[8] M A F Gomes, T I Jyh, T I Ren, I M Rodrigues, and C B S Furtado. Mechanically deformed crumpled surfaces. *Journal of Physics D: Applied Physics*, 22(8):1217–1221, aug 1989.

[9] C. C. Donato, M. A. F. Gomes, and R. E. de Souza. Crumpled wires in two dimensions. *Phys. Rev. E*, 66:015102, Jul 2002.

[10] S. Deboeuf, M. Adda-Bedia, and A. Boudaoud. Energy distributions and effective temperatures in the packing of elastic sheets. *EPL (Europhysics Letters)*, 85(2):24002, 2009.

[11] C. C. Donato, M. A. F. Gomes, and R. E. de Souza. Scaling properties in the packing of crumpled wires. *Phys. Rev. E*, 67:026110, Feb 2003.

[12] Laurent Boué and Eytan Katzav. Folding of flexible rods confined in 2d space. *EPL (Europhysics Letters)*, 80(5):54002, 2007.

[13] Y. C. Lin, Y. W. Lin, and T. M. Hong. Crumpling wires in two dimensions. *Phys. Rev. E*, 78:067101, Dec 2008.

[14] N. Stoop, F. K. Wittel, and H. J. Herrmann. Morphological phases of crumpled wire. *Phys. Rev. Lett.*, 101:094101, Aug 2008.

[15] C. C. Donato and M. A. F. Gomes. Condensation of elastic energy in two-dimensional packing of wires. *Phys. Rev. E*, 75:066113, Jun 2007.

[16] Jaime Agudo-Canalejo and Ramin Golestanian. Pattern formation by curvature-inducing proteins on spherical membranes. *New Journal of Physics*, 19(12):125013, dec 2017.

[17] B. Carneiro da Cunha. Crumpled wires and liouville field theory. *EPL (Europhysics Letters)*, 88(3):31001, 2009.

[18] T A Sobral and M A F Gomes. Tight packing of a flexible rod in two-dimensional cavities. *Journal of Physics D: Applied Physics*, 48(33):335305, 2015.

[19] T. A. Sobral and M. A. F. Gomes. Packing loops into annular cavities. *Phys. Rev. E*, 95:022312, Feb 2017.

[20] Yasuaki Morigaki, Hirofumi Wada, and Yoshimi Tanaka. Stretching an elastic loop: Crease, helicoid, and pop out. *Phys. Rev. Lett.*, 117:198003, Nov 2016.

[21] L. D. Landau and E. M. Lifshitz. *Theory of Elasticity*. Pergamon Press, 1986.

[22] Michel Nizette and Alain Goriely. Towards a classification of euler–kirchhoff filaments. *Journal of Mathematical Physics*, 40(6):2830–2866, 1999.

[23] V. G. A. Goss, G. H. M. van der Heijden, J. M. T. Thompson, and S. Neukirch. Experiments on snap buckling, hysteresis and loop formation in twisted rods. *Experimental Mechanics*, 45(2):101, 2005.

[24] F. Bosi, D. Misseroni, F. Dal Corso, and D. Bigoni. Self-encapsulation, or the 'dripping' of an elastic rod. *Proceedings of the Royal Society of London A: Mathematical, Physical and Engineering Sciences*, 471(2179), 2015.

[25] L. Boué, M. Adda-Bedia, A. Boudaoud, D. Cassani, Y. Couder, A. Eddi, and M. Trejo. Spiral patterns in the packing of flexible structures. *Phys. Rev. Lett.*, 97:166104, Oct 2006.

[26] S. Deboeuf, E. Katzav, A. Boudaoud, D. Bonn, and M. Adda-Bedia. Comparative study of crumpling and folding of thin sheets. *Phys. Rev. Lett.*, 110:104301, Mar 2013.